minerals

MDPI

Article

Evolution of Contact Metamorphic Rocks in the Zhoukoudian Area: Evidence from Phase Equilibrium Modelling

Jun Yan [1], Ying Cui [1,*] and Xiaoyu Liu [2,*]

[1] MOE Key Laboratory of Orogenic Belt and Crustal Evolution, School of Earth and Space Sciences, Peking University, Beijing 100871, China; 2201110641@pku.edu.cn
[2] National Research Center for Geoanalysis, Beijing 100037, China
* Correspondence: cuiying0430@126.com (Y.C.); liuxiaoyu0725@163.com (X.L.)

Abstract: The Yanshan intraplate tectonic belt is a tectonic-active area in the central part of the North China Craton that has undergone long-term orogenic evolution. Detailed studies on magmatic activity and metamorphism of this belt are significant for restoring its orogenic thermal evolution process. The Fangshan pluton in the Zhoukoudian area within this tectonic belt is a product of the late Mesozoic Yanshan event. However, there is a lack of detailed research on the metamorphic evolution history of the ancient terrane surrounding the Fangshan pluton subjected to contact thermal metamorphism. To further constrain the metamorphic P–T evolution of contact metamorphism associated with the Fangshan pluton, we collected rock samples in the andalusite–biotite contact metamorphic zone of the Fangshan pluton, and conducted petrographic investigations, geochemical and mineral composition analysis, and phase equilibrium modeling. The phase equilibrium modeling in the MnO–Na_2O–CaO–K_2O–FeO–MgO–Al_2O_3–SiO_2–H_2O–TiO_2–O system indicates that the peak mineral assemblages of andalusite–biotite schists are pl + q + mu + bi + and ± kfs + ilm + mt, formed at 550 to 610 °C, 1 to 3.5 kbar, and the peak mineral assemblage of garnet–andalusite–cordierite–biotite schists is gt + pl + q + bi + and + cord + ilm + mt, formed at 580 to 620 °C, 1.5 to 2.1 kbar. Therefore, we believe that the rocks in the andalusite biotite contact metamorphic zone of the Fangshan pluton underwent low pressure and medium temperature metamorphism, with the peak metamorphic conditions of about 550–610 °C, <3.5 kbar. The results show that the rocks in contact with the thermal metamorphic zone were rapidly heated by the heat released by the Fangshan pluton, and after reaching the peak metamorphic temperature, they were cooled down simultaneously with the cooling of the rock mass, defined in a nearly isobaric P–T trajectory.

Keywords: pseudosection; Zhoukoudian area; andalusite–biotite contact metamorphic zone; P–T trajectory

Citation: Yan, J.; Cui, Y.; Liu, X. Evolution of Contact Metamorphic Rocks in the Zhoukoudian Area: Evidence from Phase Equilibrium Modelling. *Minerals* **2023**, *13*, 1056. https://doi.org/10.3390/min13081056

Academic Editors: Mauricio Calderón, Jianxin Zhang and Shengyao Yu

Received: 11 June 2023
Revised: 7 July 2023
Accepted: 6 August 2023
Published: 10 August 2023

1. Introduction

The Yanshan intraplate tectonic belt is located in the central part of the North China Craton, and is an active tectonic belt reformed above the stable continent block, which has experienced a long history of orogenic evolution [1–3]. Detailed research on magmatic activity and metamorphism is of great significance for restoring the orogenic thermal evolution process of the Yanshan intraplate tectonic belt [4–6]. The Fangshan pluton in the Zhoukoudian area within the tectonic belt is a product of the late Mesozoic Yanshan movement [7–9]. Significant research results have been achieved in the petrology, magma origin and evolution, and diapir dynamics of the Fangshan pluton [10–13]. Intrusion of pluton will inevitably lead to contact metamorphism of the surrounding geological bodies [14–16]. The ancient terrane surrounding the Fangshan pluton that was subjected to contact metamorphism has also aroused wide interest. Although previous studies on geothermometry and phase equilibrium modeling of these ancient terranes have been carried out, these studies generally ignore the consideration of minor components in rock

and mineral systems, such as TiO_2, CaO, and Na_2O. More precise metamorphic research on these terranes is of necessity. Constraining the metamorphic evolution history of these ancient terranes will help to construct tectonic and thermal evolution of the Yanshan orogeny.

The metamorphism of rocks in orogenic belts is a response to thermal disturbances during the evolution of the orogenic belt [17–19]. Different P–T conditions of metamorphism reflect a specific geothermal gradient during metamorphism, while a specific geothermal gradient often corresponds to a specific tectonic background [20]. For example, high-pressure and ultra-high-pressure metamorphism is often associated with the subduction and collision orogenic belt. The study of the metamorphic processes of these rocks in orogenic belts is an important approach to help restore the evolution of orogenic belts. Conventional mineral pair geothermobarometry is generally used to calculate the temperature and pressure of metamorphism during metamorphic studies. One basic principle is that when the element exchange reaction between two minerals reaches equilibrium, there is a linear relationship between the element distribution of the mineral pairs and temperature. A typical example is a garnet–biotite thermometer, which uses Fe–Mg exchange equilibrium between garnet and biotite to calculate metamorphic temperature conditions [21]. However, during contact thermal metamorphism, it is generally the process of near isobaric heating and cooling, which occurs for a very short time. Many minerals are in a metastable state, and there is not enough time to exchange elements. The redistribution of elements between mineral pairs with temperature becomes very weak. In this case, the temperature conditions during the peak metamorphic period calculated by mineral pair equilibrium are generally lower than the actual temperature conditions, which makes it unsuitable to calculate the temperature of the contact metamorphism. In addition, in thermodynamic systems, the influence of temperature changes on mineral composition is diverse. The Ti and Al contents in biotite and Ca and Mn contents in garnet will affect the results of the garnet–biotite thermometer. For several years, using internal consistent thermodynamic databases, and related computing software THERMOCALC and Theriak-Domino, we have been able to calculate quantitatively a series of column phase diagrams including P–T projection diagrams, compatibility diagrams, and pseudosections of P–T, T–X, and P–X [22–24]. The metamorphic phase equilibrium, provides us with an efficient way to study the relationship between characteristic metamorphic mineral assemblages, metamorphic temperature and pressure conditions, and overall rock composition in metamorphic rocks [25,26]. In particular, in order to accurately and quantitatively constrain the metamorphic P–T processes, the mineral composition isopleth, mineral mole fraction isopleth, and water content isopleth can be also projected on the pseudosection [27]. Compared to conventional geothermobarometry based on ion exchange between minerals pairs, the advantage of the phase equilibrium modeling calculation is that the temperature and pressure conditions for rock formation can be well determined using single mineral composition, without considering the balance between mineral combinations [26].

In this contribution, a detailed petrographic and geochemical analysis of rocks was conducted, and then phase equilibrium modeling was used to calculate the peak metamorphic temperature of terranes in the contact metamorphic aureole around the Fangshan pluton during the Yanshan orogenic thermal evolution [28,29]. The mineral abbreviations used in the text are as follows: alm—almandine; and—andalusite; bi—biotite; chl—chlorite; cord—cordierite; grt—garnet; gro—grossular; kfs—k-feldspar; ilm—ilmenite; ky—kyanite; liq—melt; mt—magnetite; mu—muscovite; pa—paragonite; pl—plagioclase; py—pyrope; q—quartz; sill—sillimanite; sp—spessartine.

2. Geological Setting

The study area is located in the Zhoukoudian area of Beijing (Figure 1b), and the geotectonic location is located in the Yanshan intraplate tectonic zone in the middle of the North China Craton, which belongs to the border zone of the Taihang Mountains, the Yanshan Mountains, and the North China Plain (Figure 1a) [30–32]. The strata in Zhouk-

oudian and its adjacent areas are well developed in the North China Craton [33]. However, the entire stratigraphic sequence in this area has been subjected to varying degrees of metamorphism and deformation, forming the Archean metamorphic complex, Proterozoic and Paleozoic regional metamorphism, contact thermal metamorphism, and dynamic metamorphic rocks [34,35]. The Paleoproterozoic strata in the region are absent, while the Mesoproterozoic and Neoproterozoic strata are widely distributed. The Mesoproterozoic strata is mainly composed of terrigenous clastic sandstones of the Great Wall Group and tidal flat dolomite of the Jixian Group. The rocks generally undergo weak metamorphism, and some terranes are highly metamorphosed due to the intrusion of the Fangshan composite pluton. The Qingbaikou Group of the Neoproterozoic is well exposed, with a set of tidal flat and shallow marine sedimentary rocks dominated by the Lower Maling, Longshan, and Jingeryu formations. Except for the absence of the Silurian and Devonian strata since the Phanerozoic, the rest of the strata are exposed in the region.

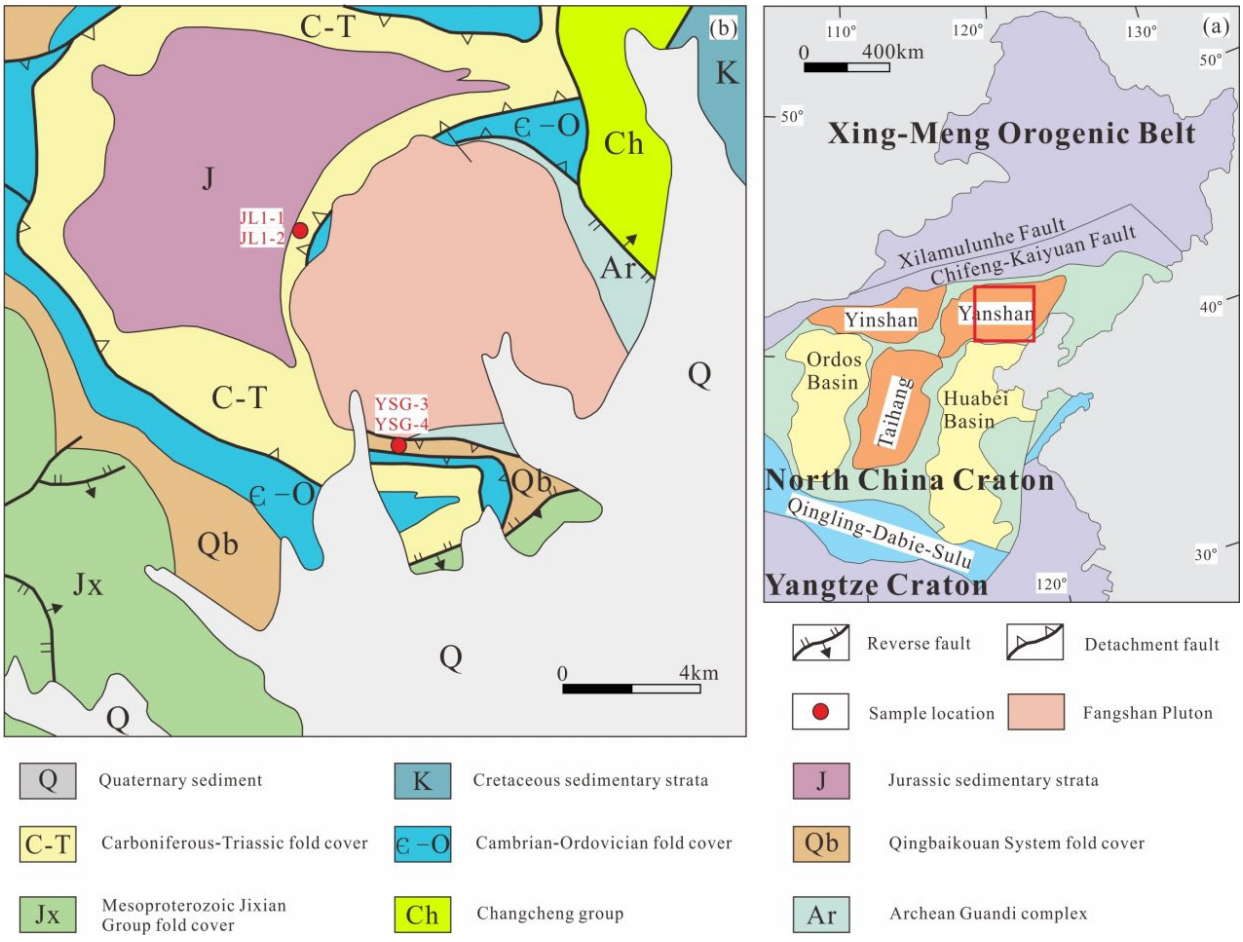

Figure 1. (**a**) Simplified geological map of the North China Craton. (**b**) Simplified geological map of the Zhoukoudian area, showing sample locations.

The magmatic activity in the region is mainly dominated by intermediate-acid magma, with the largest outcrop being the Permian Fangshan composite pluton, which is nearly circular in plane, with a diameter of 7.5 to 9 km [36,37]. The pluton is a medium-sized rock stock with relatively steep contact surface. The main lithology of the pluton is quartz monzodiorite and granodiorite [38,39]. The crystallization temperature and pressure conditions of the Fangshan pluton are constrained by 655.9–733.7 °C, 0.39–0.28 ± 0.06 GPa [40]. The oldest terrane in the domain is the Archean Guandi Complex, mainly composed of intermediate to high grade metamorphic hornblende plagioclase gneiss, gneissic migmatite, and plagioclase amphibolite, which are scattered around the Fangshan pluton [41–43]. More

than 75% of the area belongs to the Phanerozoic regional metamorphic rock outcrop area, but contact metamorphism was superimposed within the range of 1000 to 1500 m around the Fangshan composite pluton, and different metamorphic gradient zones were formed. The closer to the Fangshan pluton, the stronger is the grade of contact metamorphism. From near to far, they are, respectively, as follows: the sillimanite–K-feldspar zone, the sillimanite–muscovite zone, the garnet–staurolite zone, and the andalusite–biotite zone. The samples in this paper are all collected from the andalusite–biotite zone.

3. Field Observations and Petrography

Samples YSG-3 and YSG-4 were collected from the Guandi-Yangshigou area in the south of the Fangshan pluton (Figure 2a), located at the boundary between the Middle Proterozoic Jixian Tieling formation and the Neoproterozoic Xiamaling formation. Samples YSG-3 and YSG-4 were collected from the Neoproterozoic Xiamaling formation. Most of the contact thermal metamorphic rocks have developed foliation structures.

Sample YSG-3 is an andalusite–biotite schist, developed in a granular columnar metamorphic texture and foliation structure. The porphyroblasts are mainly euhedral andalusite (15%), in which the andalusite crystals are thick and in a short columnar shape. On the cross section of andalusite, "X-shaped" conjugated micro cracks can be seen, with some grains having an obvious zonal structure (Figure 2c). Irregular carbon inclusions are contained in the core and edge of the porphyroblasts. The foliation is defined by preferred orientation of biotites and aluminosilicates (Figure 2d). The difference from the regional metamorphic andalusite schist is that the andalusite has a larger size, a zonal structure, a polychromatic core, and a colorless andalusite without polychromism in the outer ring. Garnet is medium grained and can only be seen in some samples, distributed sporadically. The matrix is mainly composed of directionally arranged biotite, with larger biotite laths in the matrix. The sample contains a small amount of muscovite and small grains of quartz.

The mineral composition of sample YSG-4 is the same as that of YSG-3, except that the content of garnet in the former is higher (10%) compared to the latter, so it is named as garnet–andalusite–biotite schist (Figure 2e).

Samples JL1-1 and JL1-2 were collected from the Jinzushan Area (Figure 2b) in the west of the Fangshan pluton, belonging to the Hongmiaoling Formation of the Middle-Upper Permian, and also subjected to contact metamorphism of the Fangshan pluton. The sample is dark gray to black-gray in massive structure, and the andalusite porphyroblasts display a size of 2 to 8 mm, without obvious directional arrangement. Sample JL1-1 is an andalusite hornfels with porphyroblastic texture. The porphyroblasts are euhedral coarse grained andalusite, and sericitization mostly at the edges of the grains (Figure 2f). The matrix is composed of small grained felsic minerals and opaque minerals, which are cryptocrystalline, making it difficult to distinguish the specific mineral content. However, based on the mineral composition of the sample, it was determined that the protolith is a sedimentary pelitic rock.

Sample JL1-2 is garnet–andalusite–cordierite–biotite schist with porphyroblastic texture. The porphyroblasts are composed of garnet, andalusite, and cordierite. Andalusite is in a short columnar shape with a diamond-shaped cross section and contains many small mineral inclusions. Cordierite has a sieve like porphyroblastic structure (Figure 2g), its grains are heteromorphic and relatively broken, and it also contains many small inclusions of quartz and feldspar. The garnet is an idiomorphic form and experienced late retrograde metamorphism, developing metasomatic residual structures (Figure 2h). The matrix minerals are mainly biotite, felsic oriented minerals (quartz and feldspar) and a small amount of biotite undergoes retrograde metamorphism to form muscovite (sericite).

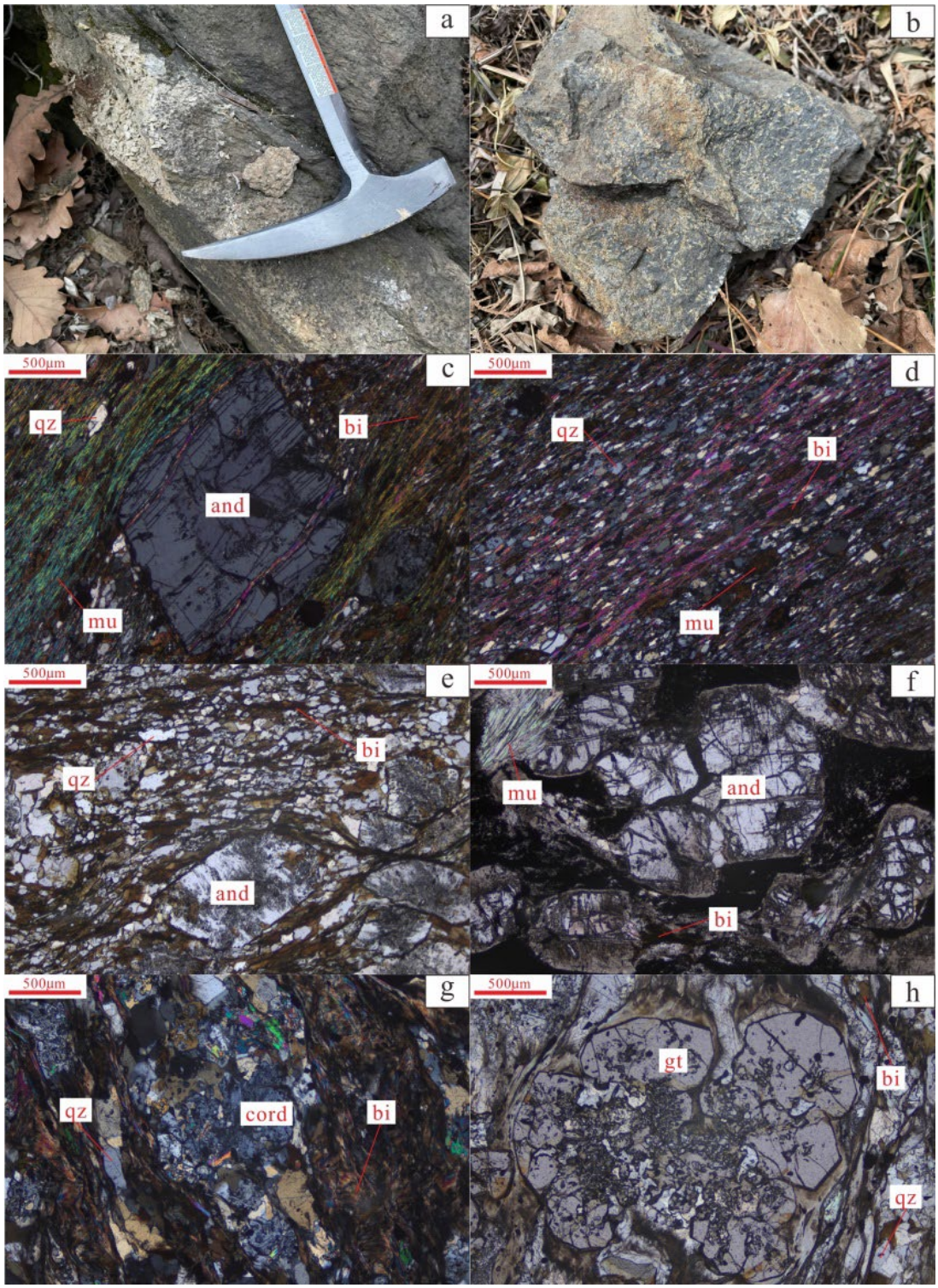

Figure 2. Field and microscopic photos of contact metamorphic rocks in Zhoukoudian area. (**a**) Field occurrence photo of andalusite–biotite schist. (**b**) Hand specimen photos of andalusite hornstones. (**c**) Andalusite porphyroblasts develop X-shaped conjugate micro fractures with zoned texture in biotite schist. (**d**) Orientation structure of andalusite–biotite schist with no S-or Z-type rotational structures developed. (**e**) Andalusite–biotite schist andalusite contains micro inclusions. (**f**) Sericite alteration of Andalusite porphyroblasts in andalusite hornstones. (**g**) Sieve like crystalloblastic texture of cordierite in garnet–andalusite–cordierite–biotite schist. (**h**) Metasomatic residual texture of garnet–andalusite–cordierite–biotite schist.

The mineral assemblages in the four samples are similar, with the main minerals being andalusite + biotite + muscovite (sericite) + quartz + garnet + cordierite. The accessory minerals are metal minerals such as magnetite and ilmenite, and both have a large amount of graphite associated with them. These graphite of various sizes are mostly in an irregular sheet shape with lamellar aggregates, which are wrapped within andalusite porphyroblasts, together with biotite, and quartz.

4. Analytical Methods

4.1. Whole-Rock Geochemistry

Four representative samples were selected for major analyses. Major elements were analyzed by inductively coupled plasma optical emission spectrometry (ICP-OES) at Langfang Chenshuo Rock and Ore Testing Technology Service Co., Ltd., Langfang, China. The instrument model is a PE 5300V from the United States.

4.2. Electron Microprobe Analysis

Garnet, feldspar, and biotite from the samples were systematically analyzed for mineral compositions. Mineral major element compositions were determined by electron microprobe analysis (EMPA) using a Jeol JXA-8230 microprobe at the Institute of Mineral Resources, Chinese Academy of Geological Sciences, Beijing, China. The testing conditions for quantitative analysis of elements were as follows: accelerated voltage of 20 kV; beam current 50 nA; spot size 1–5 μm. The analytical procedures are detailed in [44].

5. Result

5.1. Whole-Rock Major Elements

The results of whole-rock major element analysis for the four samples are listed in Supplementary Table S1. The samples have moderate SiO_2 content (49.00–63.63 wt%), higher Al_2O_3 (21.65–34.84 wt%), lower TiO_2 (0.92–1.17 wt%), CaO (0.11–0.53 wt%), MgO (0.23–1.77 wt%), Na_2O (0.15–1.62 wt%), MnO (0.01–0.21 wt%), and P_2O_5 (0.02–0.08), while the contents of TFe_2O_3 and K_2O vary greatly. Samples YSG-3 and JL1-2 have higher TFe_2O_3 content (10.3–11.10 wt%), whereas samples YSG-4 and JL1-1 have lower TFe_2O_3 content (1.41–4.82 wt%). YSG-3 and YSG-4 have higher K_2O content (3.11–4.03 wt%), while JL1-1 and JL1-2 have lower K_2O content (0.88–1.83 wt%). According to the characteristics of the sample with high Al_2O_3 and low CaO and MgO, it was determined that it belongs to metamorphic sedimentary pelitic rock.

5.2. Mineral Chemistry

As can be seen in Supplementary Table S2, major element compositions of garnet, muscovite and biotite were analyzed by electron probe in this study. The compositions of biotite in the YSG-3 sample appeared to be consistent, with TiO_2 content from 1.56 to 1.64 wt%, and the FeO content 20.67 to 22.13 wt%. The SiO_2 content in muscovite is 44.69–45.70 wt%, and the K_2O content is 10.61–10.79 wt%. The biotite in the YSG-4 sample shows lower TiO_2 content from 1.42 to 1.49 wt%, and higher FeO content from 23.13 to 26.67 wt%. The SiO_2 content in muscovite is 42.00–44.86 wt%, and the K_2O content is 9.70–10.53 wt%. The TiO_2 content of biotite in JL1-1 sample is 1.67–1.71 wt%, and the FeO content is 19.17–26.47 wt%. The SiO_2 content in Mu is 42.71–44.75%, and the K_2O content is 9.50–10.42%. The biotite in the JL1-2 sample contains the lowest TiO_2 content of 1.22–1.24 wt%, and the highest FeO content of 25.04–26.29 wt%. The composition of garnet is relatively uniform ($Alm_{96–97}Prp_{2–3}Grs_{0–1}Sps_{0–1}$), with a significant high content of FeO ranging from 41.91 to 42.43 wt%, the content of MnO_2 ranging from 0.01 to 0.09 wt%, and the content of MgO ranging from 0.65 to 0.74 wt% (Figure 3).

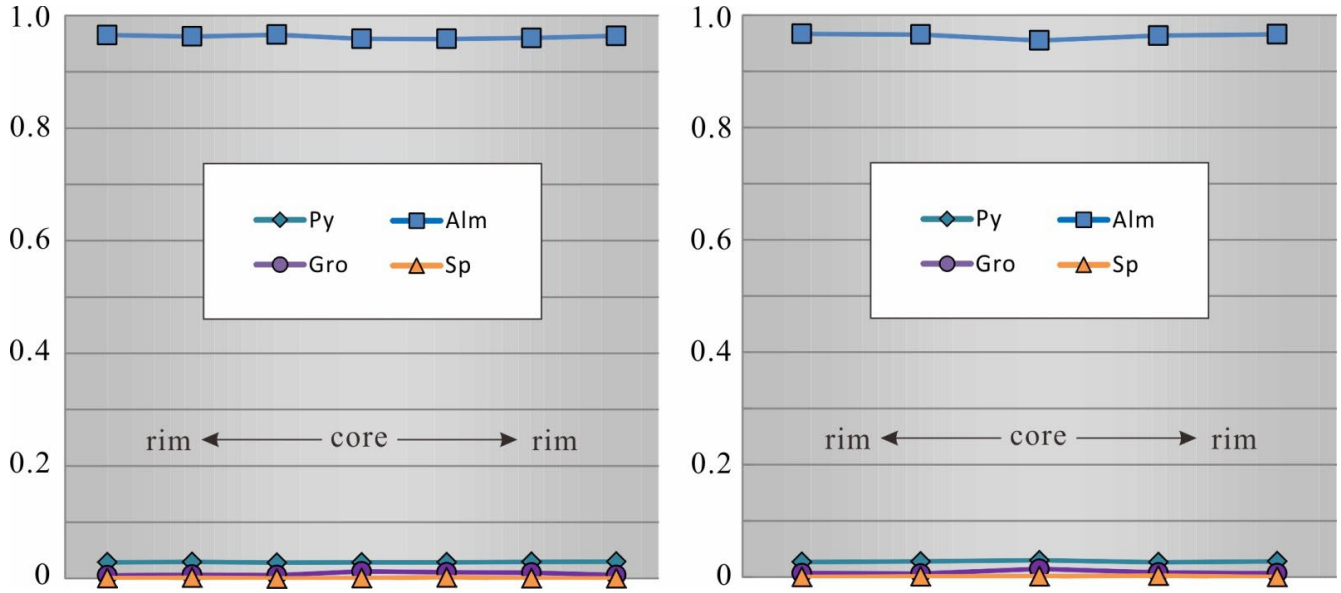

Figure 3. Composition variation diagram of garnet.

5.3. Phase Equilibrium Modeling

In this study, samples YSG-3, YSG-4, JL1-1, and JL1-2, were simulated using pseudosections to define their peak temperature and pressure conditions. The phase diagram was calculated using Theriak–Domino software [45,46] under the system of MnNCKFMASHTO ($MnO–Na_2O–CaO–K_2O–FeO–MgO–Al_2O_3–SiO_2–H_2O–TiO_2–O$). The mineral activity model of the phase diagram is based on the database of [47,48]. H_2O was assumed to be present in excess. Due to the small influence of X_{Fe3+}/X_{Fe2+} ratios on the stability domain of major mineral associations, the X_{Fe3+}/X_{Fe2+} ratios were set to 0.1. We used the whole rock major elements to conduct phase equilibrium modeling.

Figure 4a shows the phase equilibrium modeling results of YSG-3. The temperature and pressure range of the pseudosection is 450 to 700 °C at below 8 kbar. In the high temperature and low-pressure regions, biotite and muscovite will successively breakdown and disappear, while cordierite will appear in the high temperature and low-pressure regions. Due to the potassium-rich composition of the whole rock, the K-feldspar is stable over the wide range, and only breakdowns in high-temperature regions. Garnet only appears at high pressure conditions (>6 kbar). Due to the aluminum-poor composition in the whole rock composition, staurolites do not appear within the temperature and pressure range of the pseudosection. Based on our petrologic observations, the peak mineral assemblage of this sample is pl + q + kfs + mu + bi + and + ilm + mt. According to the Ti content isopleth of biotite and the K content isopleth of muscovite, they are projected into the kfs + mu + bi + and field. Referring to the EMP data, we limited the peak metamorphic temperature and pressure range to 520–610 °C, 2–3.5 kbar.

Figure 4b shows the phase equilibrium modeling results of YSG-4, with a P–T range of 450 to 700 °C and 0 to 6 kbar in the pseudosection. Compared to the YSG-3 sample, the stable temperature and pressure conditions of biotite, muscovite, garnet, and cordierite of YSG-4 have little change on the pseudosection. Unlike YSG-3, due to the low K content of the whole rock component, the stable temperature and pressure range of K-feldspar is greatly reduced, and there is no K-feldspar at both low and high temperatures. Staurolite appears at the upper left of the pseudosection (low temperature and high pressure). The peak mineral assemblage of this sample is pl + q + mu + bi + and + ilm + mt + $H_2O \pm$ gt. According to the Ti content isopleth of bi and the K content isopleth of muscovite, they are projected into the mu + bi + and + H_2O field. Referring to the EMP data, we limit the peak metamorphic temperature and pressure range to 550–610 °C and 2–3.5 kbar.

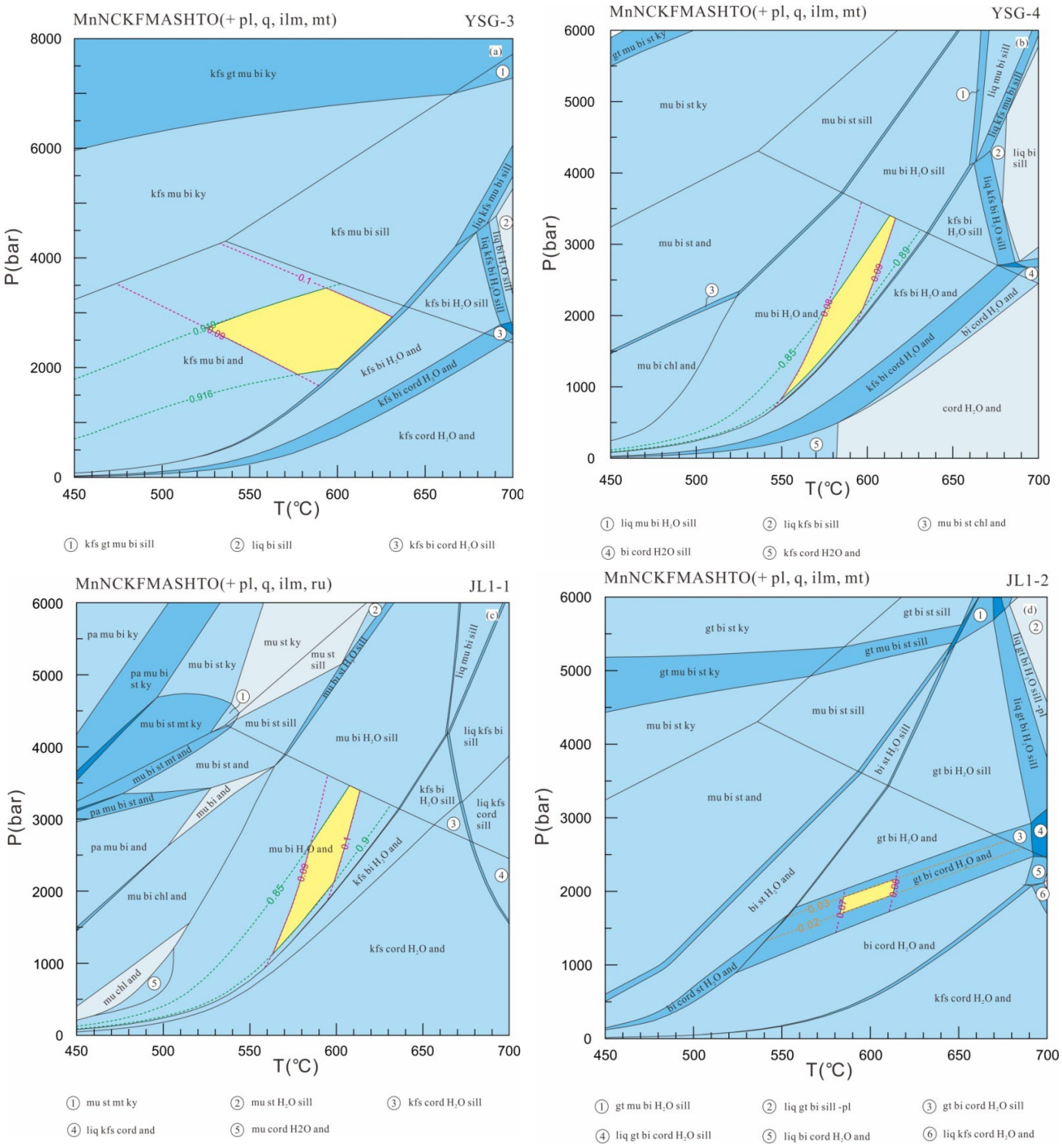

Figure 4. Phase equilibrium modeling of P–T pseudosections of sample YSG-3 (**a**), YSG-4 (**b**), JL1-1 (**c**), and JL1-2 (**d**). A few areas without marked mineral combinations can easily be inferred from the mineral combinations and degrees of freedom on both sides. The minerals after the + sign represent the excess of the mineral; (-pl) indicates that the PL is no longer excessive, and the yellow area represents the peak mineral combination. The mineral abbreviations are shown earlier. The dashed lines of purple, green, and orange represent the Ti content isopleth of biotite, the K content isopleth of muscovite and the pyrope content isopleth of garnet, respectively.

Figure 4c shows the phase equilibrium modeling results of JL1-1. The temperature and pressure range of the pseudosection is 450 to 700 °C and 0 to 6 kbar. From the pseudosection, we can see that in the high-temperature and low-pressure regions, biotite and muscovite will decompose and disappear successively, while cordierite will appear in the high-temperature and low-pressure regions. Staurolite appears at the upper left of the sectional view (low temperature and high pressure). Due to the sodium-rich content of the whole rock, paragonite may occur in the low temperature regions. The peak mineral assemblage of this sample is pl + q + mu + bi + and+ ilm + mt + H_2O. According to the Ti content isopleth of biotite and the K content isopleth of muscovite, they are projected into the mu + bi + and + H_2O field. Referring to the EMP data, we limited the peak metamorphic temperature and pressure range to 560–610 °C and 1–3.4 kbar.

Figure 4d shows the phase equilibrium modeling results of JL1-2. The temperature and pressure ranges of the pseudosection are 450 to 700 °C and 0 to 6 kbar. From the pseudosection, we can see that due to the poor potassium content of the whole rock, the stable area of muscovite is small, and it will decompose under relatively low temperature conditions. Due to the rich iron content in the whole rock, the stable range of cordierite and garnet increases, and garnet can occur under relatively low-pressure conditions. The peak mineral assemblage of this sample is gt + pl + q + bi + and + core + ilm + mt + H_2O. According to the Ti content isopleth of biotite and the pyrope content isopleth of garnet, we defined the peak metamorphic temperature and pressure range as 580–620 °C and 1.5–2.1 kbar.

6. Discussion

6.1. Metamorphic Peak Conditions and P–T Trajectory of Rock

Using the garnet–biotite thermometer [49], we obtained peak metamorphic conditions of 448–547 °C of sample JL1-2. There is an obvious difference between peak metamorphic conditions obtained from the geothermometer and the phase equilibrium modeling. This is because the garnet and biotite thermometers mainly consider the Fe–Mg exchange equilibrium, while ignoring the influence of Ti and Al contents in biotite and Ca and Mn contents in garnet on the results. This indicates that in some cases, relying solely on geothermobarometry may result in less accurate temperature and pressure conditions.

Through phase equilibrium modeling under the system of MnNCKFMASHTO, we fully considered the effects of various trace components on the system, so we can obtain more accurate temperature and pressure conditions during the metamorphic peak period. Our petrological observations and phase equilibrium modelling indicate that YSG-3, YSG-4, and JL1-1 have the same peak mineral assemblage: pl + q + mu + bi + and ± kfs + ilm + mt, formed at 520–610 °C, 1–3.5 kbar. The peak mineral assemblage of JL1-2 is gt + pl + q + bi + and + core + ilm + mt, formed at 580–620 °C and 1.5–2.1 kbar. The mineral composition analysis in the sample showed that the composition of biotite, muscovite, and garnet in the sample was relatively uniform. This indicates that the mineral assemblages of the early progressive metamorphic process were superimposed by the peak metamorphic mineral assemblages and were not preserved. Due to the fact that no progradational characteristic minerals other than peak mineral assemblages were found in the samples, the prograde metamorphic trajectory of the rock cannot be restored. We found sericitization and alteration around andalusite in the JL1-1 sample, and biotite partially transformed into muscovite (sericite) in the JL1-2 sample. As the peak metamorphic mineral assemblage of the JL1-2 sample does not include muscovite, this indicates that muscovite is a product of retrograde metamorphism after experiencing peak metamorphism.

Former literature reported the temperature and pressure conditions of rocks in different metamorphic zones in the Yitiaolong area through phase equilibrium modeling, and found that the peak temperature and pressure conditions of garnet–K-feldspar–sillimanite–biotite schists in the sillimanite zone were P = 3.9–4.1 kbar, T = 690 °C. The metamorphic peak temperature and pressure conditions of the garnet–andalusite–staurolite–mica schist in the garnet–staurolite zone were determined as P = 3.6–3.7 kbar, T = 580–590 °C [40]. The

metamorphic peak temperature and pressure conditions of the andalusite–biotite schist in the andalusite zone were P = 3.2–3.6 kbar, T = 580–590 °C, and the rock undergoes a metamorphic P–T trajectory of near isobaric heating and isobaric cooling [50,51]. In addition, the mineral assemblages in the pseudosection (pelitic rock in the KFMASH system) where the metamorphic P-T trajectory is located are andalusite, biotite, muscovite, and quartz, which are consistent with the mineral assemblages of the three samples in this study. The peak metamorphic condition is constrained to P < 4 kbar, T = 530–625 °C. This is consistent with the peak metamorphic temperature and pressure conditions of 550–610 °C, 1–3.5 kbar and 580–620 °C, 1.5–2.1 kbar calculated by our phase equilibrium modeling. Compared with the phase equilibrium modeling under the typical KMnFMASH system in former literature, the phase equilibrium modeling in this study adds CaO, Na_2O, and TiO_2 components, which control the composition of plagioclase, biotite, and garnet in the mineral assemblage. This makes the calculated peak metamorphic conditions more accurate and convincing. Due to the relatively uniform composition of the main minerals in the rocks, it is difficult to determine the prograde and post-peak retrogressive metamorphic trajectory of the rock solely based on the phase equilibrium modeling. However, according to the calculation results of the carbon based Raman spectrum thermometer we carried out for the rocks previously [52], the core of the andalusite porphyroblasts of rocks in the andalusite–biotite zone around the Fangshan pluton recorded a metamorphic temperature during the early progressive metamorphic process (~550 °C), and the peak metamorphic temperature conditions (~598 °C) were recorded by the edges of andalusite porphyroblasts [52]. The rock matrix may have recorded the post-peak retrogressive metamorphic temperature of 598–574 °C. Therefore, we believe that the rocks in the andalusite–biotite contact metamorphic aureole of the Fangshan pluton underwent low pressure and medium temperature metamorphism, with peak metamorphic conditions of about 550–610 °C, <3.5 kbar.

6.2. Tectonic Implication

The Zhoukoudian area is located in the Yanshan Intraplate Tectonic Belt, which was affected by the Yanshan event during the Mesozoic era [53,54]. With different tectonic movements, two large-scale metamorphisms occurred in the area. The Fangshan pluton was emplaced during the late Yanshan event, and is mainly composed of quartz monzodiorite and granodiorite [55]. Based on an amphibole plagioclase thermometer and an amphibole total Al-content geobarometer, previous researchers calculated the temperature and pressure of the Fangshan pluton during intrusion. The crystallization temperature and pressure conditions of the Fangshan pluton are constrained of 655.9–733.7 °C, 0.39–0.28 ± 0.06 GPa [40]. Regarding the dynamic mechanism of emplacement of the Fangshan pluton, most of the predecessors tended to believe that the magma emplacement mechanism is balloon-inflation intrusion, whereas some researchers prefer the magma diapir mechanism. There is reason to believe that the intrusion of the Fangshan pluton inevitably led to the occurrence of tectonic deformation and contact thermal metamorphism of the peripheral terranes.

The foliation relationship between the metamorphic porphyroblasts and the matrix in contact with metamorphic wall rocks can be used to determine the emplacement mechanism of intrusions. The andalusite porphyroblasts in andalusite–biotite schists develop X-shaped conjugate micro fractures with straight fracture boundaries (Figure 2c). The directional arrangement structure composed of biotite and muscovite in the matrix (Figure 2d) is also dominated by a flat type, with no developed S-or Z-type rotational structures. This indicates that the strain type of rock is not shear deformation, but mainly compressive deformation. This is consistent with the previous view that the magma emplacement mechanism of the Fangshan pluton is the balloon expansion type [9,50].

Based on the accurate results from phase equilibrium modeling calculations, the andalusite–biotite zone is believed to have undergone contact metamorphism. Due to the rapid heating of the rocks in the contact metamorphic zone by the heat released by the

pluton, they reached the peak metamorphic temperature and then cooled down with the cooling of the Fangshan pluton, resulting in retrograde metamorphism, forming a P–T trajectory characterized by isobaric heating and cooling.

7. Conclusions

(1) The phase equilibrium modeling of rocks in the andalusite biotite contact metamorphic zone of the Fangshan pluton indicates that the peak mineral assemblages of andalusite–biotite schists are pl + q + mu + bi + and ± kfs + ilm + mt, formed at 550–610 °C, 1–3.5 kbar, and the peak mineral assemblage of the garnet–andalusite–cordierite–biotite schists is gt + pl + q + bi + and + core + ilm + mt, formed at 580–620 °C, 1.5–2.1 kbar.

(2) The andalusite–biotite zone is believed to have undergone contact thermal metamorphism, and the peak metamorphic temperature and pressure conditions were 550–610 °C, <3.5 kbar by means of phase equilibrium modeling. Due to the influence of the Fangshan pluton, the rock recorded a P–T trajectory characterized by isobaric heating and cooling, reflecting a response to thermal disturbances caused by magmatic activity.

Supplementary Materials: The following supporting information can be downloaded at: https://www.mdpi.com/article/10.3390/min13081056/s1, Table S1: Whole-rock major element concentrations (wt%) of the contact metamorphic rock in the Zhoukoudian; Table S2: Representative compositions (wt%) of rock-forming minerals of the contact metamorphic rock in the Zhoukoudian.

Author Contributions: Conceptualization, J.Y. and Y.C.; methodology, J.Y.; software, J.Y.; formal analysis, J.Y.; investigation, J.Y. and Y.C.; resources, J.Y. and Y.C.; data curation, J.Y.; writing—original draft preparation, J.Y.; writing—review and editing, J.Y., X.L. and Y.C.; All authors have read and agreed to the published version of the manuscript.

Funding: This research received no external funding.

Data Availability Statement: The data that support the findings of this study are available from the corresponding author, Ying Cui, upon reasonable request.

Acknowledgments: We thank Zhenyu Chen and Xiaodan Chen for their help with electron probe analyses. We are also grateful to Cong Zhang and Tao Wen for their assistance.

Conflicts of Interest: The authors declare no conflict of interest.

References

1. Liu, D.Y.; Nutman, A.P.; Compston, W.; Wu, J.S.; Shen, Q. Remnants of ≥3800 Ma crust in the Chinese part of the Sino-Korean craton. *Geology* **1992**, *20*, 339–342. [CrossRef]
2. Zhao, G.; Wilde, S.A.; Cawood, P.A.; Sun, M. Archean blocks and their boundaries in the North China Craton: Lithological, geochemical, structural and P–T path constraints and tectonic evolution. *Precambrian Res.* **2001**, *107*, 45–73. [CrossRef]
3. Wong, W.H. The Mesozoic Orogenic Movement in Eastern China. *Bull. Geol. Soc. China* **1927**, *8*, 33–44. [CrossRef]
4. Dong, S.; Zhang, Y.; Long, C.; Yang, Z.; Ji, Q.; Wang, T.; Hu, J.; Chen, X. Jurassic Tectonic Revolution in China and New Interpretation of the Yanshan Movement. *Acta Geol. Sin* **2007**, *81*, 1449–1461.
5. Hao, W.; Zhu, G.; Zhu, R. Timing of the Yanshan Movement: Evidence from the Jingxi Basin in the Yanshan fold-and-thrust belt, eastern China. *Int. J. Earth Sci.* **2019**, *108*, 1961–1978. [CrossRef]
6. Yang, J.; Wu, F.; Shao, J.; Wilde, S.; Xie, L.; Liu, X. Constraints on the timing of uplift of the Yanshan Fold and Thrust Belt, North China. *Earth Planet. Sci. Lett.* **2006**, *246*, 336–352. [CrossRef]
7. Feng, Q.; Qiu, N.; Chang, J.; Liu, N. Tectonothermal Evolution of the Fangshan pluton: Constraints from the (U-Th)/He Ages. *Earth Sci.-J. China Univ. Geosci.* **2018**, *43*, 1972–1982. [CrossRef]
8. He, B.; Xu, Y.; Wang, Y.; Wei, B. Magmatic Diapir of Fangshan Pluton in the Western Hills, Beijing and Its Geological Significance. *Earth Sci.-J. China Univ. Geosci.* **2005**, *30*, 298–308.
9. Ma, C. The magma-dynamic mechanism of emplacement and compositional zonation of the Zhoukoudian stock, Beijing. *Acta Geol. Sin.* **1988**, *4*, 329–341.
10. Cai, J.; Yan, G.; Mu, B.; Ren, K.; Song, B.; Li, F. Zircon U-Pb age, Sr-Nd-Pb isotopic compositions and trace element of Fangshan complex in Beijing and their petrogenesis significance. *Acta Geol. Sin.* **2005**, *21*, 776–788.
11. He, B.; Xu, Y.-G.; Paterson, S. Magmatic diapirism of the Fangshan pluton, southwest of Beijing, China. *J. Struct. Geol.* **2009**, *31*, 615–626. [CrossRef]

12. Sun, J.-F.; Yang, J.-H.; Wu, F.-Y.; Li, X.-H.; Yang, Y.-H.; Xie, L.-W.; Wilde, S.A. Magma mixing controlling the origin of the Early Cretaceous Fangshan granitic pluton, North China Craton: In situ U–Pb age and Sr-, Nd-, Hf- and O-isotope evidence. *Lithos* **2010**, *120*, 421–438. [CrossRef]
13. Zhang, Z.-K.; Ling, M.-X.; Zhang, L.-P.; Sun, S.-J.; Sun, W. Pluton incremental growth by multi-stage magma pulsations: Evidence from the Fangshan pluton, North China Craton. *Tectonophysics* **2022**, *838*, 229480. [CrossRef]
14. Ahmed, A.H.; Surour, A.A. Fluid-related modifications of Cr-spinel and olivine from ophiolitic peridotites by contact metamorphism of granitic intrusions in the Ablah area, Saudi Arabia. *J. Asian Earth Sci.* **2016**, *122*, 58–79. [CrossRef]
15. Costamagna, L.G.; Elter, F.M.; Gaggero, L.; Mantovani, F. Contact metamorphism in Middle Ordovician arc rocks (SW Sardinia, Italy): New paleogeographic constraints. *Lithos* **2016**, *264*, 577–593. [CrossRef]
16. Sklyarov, E.V.; Lavrenchuk, A.V.; Fedorovsky, V.S.; Gladkochub, D.P.; Donskaya, T.V.; Kotov, A.B.; Mazukabzov, A.M.; Starikova, A.E. Regional, Contact Metamorphism, and Autometamorphism of the Olkhon Terrane (West Baikal Area). *Petrology* **2020**, *28*, 47–61. [CrossRef]
17. Kang, W.; Li, W.; Dong, Y.; Zhang, L.; Zhao, J.; Sheir, F. Multi-stage metamorphism and deformation of the North Qinling Orogenic Belt: Constraints from petrology, geochronology, and structural analysis of the Qinling Complex. *Gondwana Res.* **2022**, *105*, 201–216. [CrossRef]
18. Li, Z.M.G.; Chen, Y.-C.; Zhang, Q.W.L.; Liu, J.-H.; Wu, C.-M. P-T conditions and timing of metamorphism of the Yuanmou area, southern Neoproterozoic Kang-Dian Orogenic Belt, southwest China. *Precambrian Res.* **2022**, *374*, 106642. [CrossRef]
19. Spear, F.S. *Metamorphic Phase Equilibria and Pressure-Temperature-Time Paths*; Mineralogical Society of America: Chantilly, VA, USA, 1993.
20. Brown, M. Duality of thermal regimes is the distinctive characteristic of plate tectonics since the Neoarchean. *Geology* **2006**, *34*, 961–964. [CrossRef]
21. Wei, C.; Su, X.; Lou, Y.; Li, Y. A new interpretation of the conventionnal ther mobarometry in the eclgite: Evidence from the calculated PT pseudosection. *Acta Petrol. Sin.* **2009**, *25*, 2078–2088.
22. Guo, Y.; Zhao, G.; Guo, R.; Han, Y.; Wei, Z.; Zhou, N.; Ju, P. Late Paleoproterozoic orogenic evolution of the northern Tarim Craton, NW China: Insights from phase equilibrium modeling and zircon U-Pb geochronology of metapelitic granulite in the Kuluketage area. *Gondwana Res.* **2022**, *106*, 351–366. [CrossRef]
23. Otto, T.; Stevens, G.; Mayne, M.J.; Moyen, J.-F. Phase equilibrium modelling of partial melting in the upper mantle: A comparison between different modelling methodologies and experimental results. *Lithos* **2023**, *444–445*, 107111. [CrossRef]
24. Wei, C.; Zhu, W. Granulite facies metamorphism and petrogenesis of granite (I): Metamorphic phase equilibria for HT-UHT metapelites/greywackes. *Acta Petrol. Sin.* **2016**, *32*, 1611–1624.
25. Faryad, S.W.; Jezek, J.; Connolly, J.A.D. Advantages and limitations of combined diffusion-phase equilibrium modelling for pressure-temperature-time history of metamorphic rocks. *J. Petrol.* **2022**, *63*, egac118. [CrossRef]
26. Wei, C. Approaches and advancement of the study of metamorphic p-T-t paths. *Earth Sci. Front.* **2011**, *18*, 1–16.
27. Wei, C.; Zhou, X. Process in The Study of Metamorphic Phase Equilibrium. *Earth Sci. Front.* **2003**, *10*, 341–351.
28. Lin, W.; Faure, M.; Chen, Y.; Ji, W.; Wang, F.; Wu, L.; Charles, N.; Wang, J.; Wang, Q. Late Mesozoic compressional to extensional tectonics in the Yiwulüshan massif, NE China and its bearing on the evolution of the Yinshan-Yanshan orogenic belt: Part I: Structural analyses and geochronological constraints. *Gondwana Res.* **2013**, *23*, 54–77. [CrossRef]
29. Zhang, Y.; Yuan, X.; Wang, M.; Ge, P.; Yancui, H.; Xu, J.; Zhang, J.; Cheng, J.; Jiang, Z. Discovery of lacustrine shale deposits in the Yanshan Orogenic Belt, China: Implications for hydrocarbon exploration. *Geosci. Front.* **2021**, *12*, 101256. [CrossRef]
30. Davis, G.A.; Yadong, Z.; Cong, W.; Darby, B.J.; Changhou, Z.; Gehrels, G.E. Mesozoic tectonic evolution of the Yanshan fold and thrust belt, with emphasis on Hebei and Liaoning provinces, northern China. *Geol. Soc. Am. Mem.* **2001**, *194*, 171–197.
31. Liu, S.; Zhang, A.; Lin, C.; Zhang, B.; Yuan, H.; Huang, D.; Steel, R.J.; Horton, B.K. Thrust duplexing and transpression in the Yanshan Mountains: Implications for early Mesozoic orogenesis and decratonization of the North China Craton. *Basin Res.* **2021**, *33*, 2303–2327. [CrossRef]
32. Zeng, J.P.; Wei, W.; Lin, W.; Meng, L.; Qiu, H.; Chu, Y.; Ren, Z.; Wang, Y.; Feng, Z.; Li, Q.; et al. The Late Jurassic extensional event in the Yanshan fold and thrust belt (North China): New insights from an integrated study of structural geology, geophysics, and geochemistry of the Siganding granitic pluton. *J. Asian Earth Sci.* **2021**, *211*, 104708. [CrossRef]
33. Wang, C.; Wang, X.; Chen, J. Digital Geological Mapping to Facilitate Field Data Collection, Integration, and Map Production in Zhoukoudian, China. *Appl. Sci.* **2021**, *11*, 5041. [CrossRef]
34. Liu, B.; Ba, J.; Zhang, L.; Chen, N.; Li, X.; Zhang, Z.; Chen, H.; Yuan, Y. Zircon LA-ICP-MS U-Pb Dating of Metamorphism and Anatexis of the Guandi Complex, Zhoukoudian Area, Beijing. *Geol. Sci. Technol. Inf.* **2008**, *27*, 37–42.
35. Song, H.; Ge, M. The Indosinian Movement in the Western Hill of Beijing Discussed in the Light of the Structural Characteristics. *Geol. Rev.* **1984**, *30*, 77–88.
36. Xu, H.; Song, Y.; Ye, K.; Zhang, J.; Wang, H. Petrogenesis of mafic dykes and high-Mg adakitic enclaves in the Late Mesozoic Fangshan low-Mg adakitic pluton, North China Craton. *J. Asian Earth Sci.* **2012**, *54*, 143–161. [CrossRef]
37. Yan, D.-P.; Zhou, M.-F.; Zhao, D.; Li, J.; Wang, G.; Wang, C.; Qi, L. Origin, ascent and oblique emplacement of magmas in a thickened crust: An example from the Cretaceous Fangshan adakitic pluton, Beijing. *Lithos* **2011**, *123*, 102–120. [CrossRef]
38. Liu, F.; Zhang, Z.; Zhang, Z.; Li, X.; Yang, D. Ca isotopic compositions of zoned granitoid intrusion: Implications for the emplacement and evolution of magma bodies. *Geochim. Cosmochim. Acta* **2022**, *326*, 149–165. [CrossRef]

39. Zhang, J.; Ma, C.; Zhang, C.; Li, J. Fractional crystallization and magma mixing: Evidence from porphyritic diorite-granodiorite dykes and mafic microgranular enclaves within the Zhoukoudian pluton, Beijing. *Mineral. Petrol.* **2014**, *108*, 777–800. [CrossRef]
40. Liu, X.; Cheng, S.; Zhang, H. Polybaric Crystallization of Granitic Magmas and Its Dynamic Significance: A Case from the Fangshan Pluton of Beijing. *Geoscience* **2015**, *29*, 514–528.
41. Yan, D.-P.; Zhou, M.-F.; Song, H.; Wang, G.; Sun, M. Mesozoic extensional structures of the Fangshan tectonic dome and their subsequent reworking during collisional accretion of the North China Block. *J. Geol. Soc.* **2006**, *163*, 127–142. [CrossRef]
42. Zhang, J.; Ma, C.; Wang, R.; Tao, J. Mineralogical, Geochronological and Geochemical Characteristics of Zhoukoudian Intrusion and Their Magmatic Source and Evolution. *Earth Sci.-J. China Univ. Geosci.* **2013**, *38*, 68–86.
43. Zhong, Y.; He, C.; Chen, N.; Xia, B.; Zhou, Z.; Chen, B.-C.; Wang, G. Tectonothermal Records in Migmatite-Like Rocks of the Guandi Complex in Zhoukoudian, Beijing: Implications for Late Neoarchean to Proterozoic Tectonics of the North China Craton. *J. Earth Sci.* **2018**, *29*, 1254–1275. [CrossRef]
44. Li, X.; Zhang, L.; Wei, C.; Slabunov, A.I.; Bader, T. Quartz and orthopyroxene exsolution lamellae in clinopyroxene and the metamorphicP-Tpath of Belomorian eclogites. *J. Metamorph. Geol.* **2018**, *36*, 1–22. [CrossRef]
45. De Capitani, C.; Brown, T.H. The computation of chemical equilibrium in complex systems containing non-ideal solutions. *Geochim. Cosmochim. Acta* **1987**, *51*, 2639–2652. [CrossRef]
46. De Capitani, C.; Petrakakis, K. The computation of equilibrium assemblage diagrams with Theriak/Domino software. *Am. Mineral.* **2010**, *95*, 1006–1016. [CrossRef]
47. Holland, T.J.B.; Powell, R. An improved and extended internally consistent thermodynamic dataset for phases of petrological interest, involving a new equation of state for solids. *J. Metamorph. Geol.* **2011**, *29*, 333–383. [CrossRef]
48. White, R.W.; Powell, R.; Holland, T.J.B.; Johnson, T.E.; Green, E.C.R. New mineral activity–composition relations for thermodynamic calculations in metapelitic systems. *J. Metamorph. Geol.* **2014**, *32*, 261–286. [CrossRef]
49. Ferry, J.M.; Spear, F.R. Experimental calibration of the partitioning of Fe and Mg between biotite and garnet. *Contrib. Mineral. Petrol.* **1978**, *66*, 113–117. [CrossRef]
50. Chen, N.; Chen, B.; Roger, M.; Yang, T.; Xia, B.; Liu, R.; Wang, G.; Xu, R. Using Contact Metamorphic Criteria in Contact Aureole to Preliminarily Discriminate Magma Emplacement Mechanisms of Fangshan Pluton, Beijing. *Earth Sci.* **2018**, *43*, 99–108.
51. Wan, Y.; Wang, G.; Guo, C.; Yu, H.; Zhang, J. Deformation features of andalusite in tectonic schist of the Xiamaling Formation of the Qingbaikouan System on the southern side of the Fangshan pluton in the Western Hills, Beijing, China. *Geol. Bull. China* **2007**, *26*, 200–205.
52. Jun, Y.; Ying, C.; Cong, Z. Evolution of contactolite in Zhoukoudian area: Evidence from carbon Raman spectrum thermometer. *Acta Mineral. Sin.* **2023**, *43*, 1–12. [CrossRef]
53. Xu, T.; Ai, Y.; Wang, G. Structural Deformation in the East Ridge of Huangyuan, Zhoukoudian and Its Geological Significance. *Geoscience* **2013**, *27*, 288–293.
54. Zhang, X.; Hu, L.; Ji, M.; Liu, J.; Song, H. Microstructures and deformation mechanisms of hornblende in Guandi complex, the Western Hills, Beijing. *Sci. China Earth Sci.* **2013**, *56*, 1510–1518. [CrossRef]
55. Qin, F.; Xu, X.; Luo, Z. Mixing and mingling in petrogenesis of the Fangshan intrusion, Beijing. *Acta Petrol. Sin.* **2006**, *22*, 2957–2970.